Influence of plastic deformation on single-fiber push-out tests of carbon fiber reinforced epoxy resin

J. Jäger, M.G.R. Sause *, F. Burkert, J. Moosburger-Will, M. Greisel, S. Horn

Experimental Physics II, Institute of Physics, University of Augsburg, 86135 Augsburg, Germany

Keywords:
A. Polymer-matrix composites (PMCs)
B. Plastic deformation
C. Micro-mechanics

A B S T R A C T

In our study we present a procedure to measure and analyze single-fiber push-out force–displacement curves on carbon fiber reinforced polymers using a cyclic loading–unloading scheme. The measured cyclic force–displacement curves allow an energy-based evaluation of the interfacial failure, taking into account elastic, plastic and other dissipative energy contributions. Experimental and modeling results demonstrate that a deviation of the push-out curve from linear behavior does not correspond to crack opening but to a plastic deformation of the matrix. Evaluating the plastic energy yields a linear increase of the total plastic energy after a certain indenter displacement. This linear increase is attributed to stable crack propagation. Back-extrapolation of the linear part to zero total plastic energy using a linear regression yields the initiation of crack growth. It is concluded that for ductile matrix materials like polymers, a reliable interpretation of push-out data has to take into account plastic material deformation.

1. Introduction

Fiber–matrix adhesion is one of the key parameters for the mechanical performance of carbon fiber reinforced polymers (CFRP). Before a specific improvement of the fiber–matrix adhesion can be addressed, a characterization and quantification of the mechanical properties of the interface is required. So far mostly macromechanical tests with a shear loading of the fiber matrix interface are performed for this purpose, e.g., tests of the interlaminar shear strength (ILS). Although such tests deliver characteristic values for macroscopic samples, they average over different modes of failure and the inhomogeneity of the sample and, therefore, do not characterize the pure fiber–matrix adhesion.

To overcome this problem micromechanical tests, like the single-fiber pull-out test [1,2], the microbond test [3,4] or the fragmentation test [5,6] have been established. The specific values obtained from these tests characterize the fiber–matrix adhesion directly, but the tests have to be performed on model composites. A direct transfer of the measured quantities to realistic, macroscopically manufactured composites is questionable. An alternative is the single-fiber push-out test, which allows a micromechanical characterization of the fiber–matrix adhesion on industrially manufactured composites. During a single-fiber push-out experiment an individual fiber within a thin, plane-parallel composite sample (thickness below 100 μm), is loaded by a diamond indenter tip. With increasing load an evolution from crack-initiation, fiber–matrix debonding to fiber push-out occurs. During the experiment, the force–displacement curve is recorded, which allows to extract values to quantify the fiber–matrix adhesion.

Fig. 1 shows schematic push-out force–displacement curves of a ceramic matrix composite (a), of a polymer matrix composite (b), and the effect of the indenter hitting the matrix surrounding the fiber (c).

The force–displacement curve measured on ceramic matrix composites initially shows a nonlinear increase of force, which results from the formation of a stable contact area between indenter and fiber (cf. Fig. 1a). After this initial stage, a linear force–displacement relation is observed. This is generally interpreted as elastic deformation of the fiber–matrix system. A further increase of the indenter displacement results in a sharp change of slope, indicating crack initiation, followed again by a linear increase of force interpreted as stable crack growth [14,15] until maximum load is reached.

For fiber reinforced polymers an initial non-linear force increase is followed by a linear force–displacement relation (cf. Fig. 1b). In contrast to ceramic matrix composites, a further increase of the indenter displacement results in a gradual change to non-linear behavior in the majority of cases. The onset of this non-linearity is often interpreted as crack initiation followed by crack growth [7–11]. Various models were proposed to deduce the interfacial shear strength based on this non-linear behavior [9–12]. Most of

* Corresponding author. Tel.: +49 821 598 3238.
E-mail address: markus.sause@physik.uni-augsburg.de (M.G.R. Sause).

the analytical models rely on assumptions concerning the stress distribution along the interface and, therefore, are restricted to special push-out geometries and types of loading. Such use of stress based values to characterize the fiber–matrix adhesion only allows a comparison of push-out tests using a similar experimental setup (e.g., same indenter geometries). This limitation can be overcome following the approach of e.g., Ref. [13] or Ref. [7] which is based on fracture mechanics to calculate a fiber–matrix adhesive energy. All these models assume that crack initiation occurs when a deviation of the force displacement curve from linear behavior is observed. The potential contributions of other dissipative mechanisms, e.g., plastic deformation of fiber or matrix, are not taken into account. This can be a valid approach to describe brittle systems like ceramic matrix composites. For carbon fiber reinforced polymers, however, the appearance of a plastic energy contribution is likely, since polymers typically show significant plastic deformation before failure. After the onset of non-linear behavior in CFRP, an increase of force up to peak load is observed [8,10,13,16].

Immediately after the peak load is reached some fiber reinforced systems show an abrupt decrease of load [7,17]. For other systems a gradual decrease of load is reported [14,18,19]. In both cases the load maximum is associated with a complete debonding of fiber and matrix followed by a push-out of the fiber. Load and indenter displacement at fiber push-out are important input parameters for several evaluation methods presented in literature. In some approaches the interfacial shear strength is evaluated based on a simple balance of force at the moment of push-out [8,15,17,20]. The values of indenter displacement and force at push-out are also required for energy based approaches, e.g., to determine the fracture toughness [14].

To ensure a reliable interpretation of a single-fiber push-out experiment contact between indenter and the matrix surrounding the fiber has to be avoided, since such contact to the matrix causes a superposition of different loading effects [8,14,15,20]. In the force–displacement curves a strong increase of load at indenter-matrix contact is observed (cf. Fig. 1c).

In the presented study we describe an experimental procedure to measure and analyze single-fiber push-out force–displacement curves using a cyclic loading–unloading scheme following the approach introduced by Refs. [14,25,27]. The resulting cyclic force–displacement curves allow an energy-based evaluation of the push-out test, taking into account elastic, plastic and further dissipative energy contributions during interfacial failure. Finite element simulations and microscopy measurements are used to back up the interpretation of the push-out experiment. The method of evaluation presented is independent of the specific shape of the force–displacement curve and is applicable to all fiber–matrix systems. Based on the experimental data obtained we are able to determine the force at crack initiation and the fracture energy dissipated during a push-out experiment. The experimental and simulation results emphasize the significance of plastic deformations of the polymeric matrix during push-out tests on CFRP and the necessity to take these effects into account to model failure behavior in polymeric composite materials.

2. Samples

The sample investigated is a carbon fiber reinforced polymer laminate containing HTA fibers (company: TohoTenax) and a RTM6 epoxy resin matrix (company: Hexcel). The resin is completely cured using a standard curing cycle (0.5 h at 120 °C, 2.5 h at 180 °C). Using a precision low speed diamond saw the resulting CFRP sample has been cut into thin slices (dimension 1 cm × 0.5 mm × 0.5 mm) with fibers aligned perpendicular to the cut face. These slices have then been lapped from both sides using a silicon carbide suspension (grain size: 3 μm), to achieve a plane parallel sample of a final thickness of 45 μm. In removing the outer 220–230 μm of sample material on each side it can be ensured that there is no residual damage introduced by the previous cutting process. The front and back surface of the 45 μm slice were finally polished with a SiO_2-suspension (grain size: 15 nm). The roughness R_a of the polished sample was quantified by atomic force microscopy (AFM) to be less than 100 nm. For the push-out experiments, the outer part of the sample is mounted with hot wax on a cleaned glass substrate. During cooling the sample is pressed onto the glass substrate to achieve full contact. The glass substrate itself contains a 50 μm wide groove positioned underneath the fibers investigated.

3. Experimental

3.1. Push-out measurements

The push-out experiments have been performed utilizing an *Universal Nanomechanical Tester* (UNAT) from ASMEC in combination with a diamond flat cone indenter (diameter at the top ~4.8 μm, Fig. 2). Compared to a standard Berkovich indenter, the flat end cone indenter has a much steeper opening angle. As was shown in a previous work, this effectively avoids hitting the matrix surrounding the fiber investigated during a push-out experiment [14]. The lateral positioning accuracy of the indenter is ±1 μm. For microscopic analysis of the push-out progress, standard push-out tests, i.e., tests using a displacement controlled loading rate of 40 nm/s up to push-out, have been stopped and unloaded at different stages of the push-out test, namely indenter displacements of

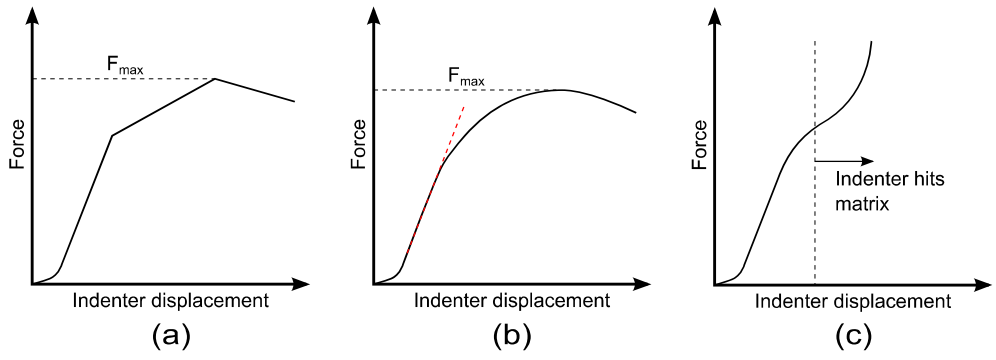

Fig. 1. Schematic force–displacement curves of: (a) push-out test of a ceramic matrix composite, (b) push-out test of a polymer-matrix composite, and (c) push-out test of a polymer matrix composite with the indenter hitting the matrix. (For interpretation of the references to color in this figure legend, the reader is referred to the web version of this article.)

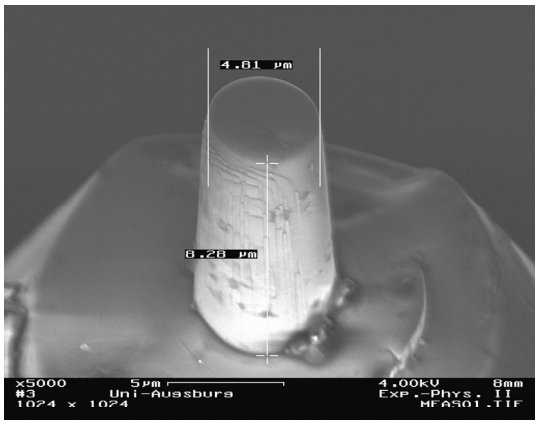

Fig. 2. Scanning electron microscopy image of the flat cone indenter as used for the push-out measurements. The top diameter is approximately 4.8 µm.

200 nm, 450 nm, 600 nm, 700 nm, 800 nm, 900 nm, and 1100 nm. These so called indentation depths are marked in the exemplary push-out force–displacement curve shown in Fig. 3. The pushed and then unloaded fibers are used to measure the residual plastic deformation of the fiber–matrix system after loading and unloading by AFM. To ensure adequate statistics, eight fibers have been tested for each indentation depth.

We performed cyclic push-out tests to obtain the different energy contributions dissipated during a push-out test (see Fig. 4). This was done by adding unloading–loading cycles after every 100 nm of indenter displacement to the standard loading curve maintaining the displacement controlled mode with a loading and unloading rate of 25 nm/s.

3.2. AFM measurements

AFM measurements were performed utilizing a Dimension ICON from Bruker, operating in standard tapping mode. The scan size of the images was 80 µm × 80 µm with a scan rate of 0.1 Hz and 1024 samples per line. To identify the residual plastic deformation of the unloaded fiber–matrix system after different indentation depths, the front and back surface of the sample have been scanned before and after the stopped push-out tests.

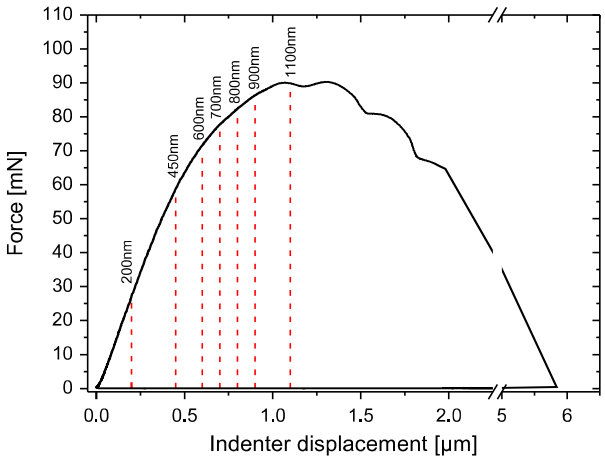

Fig. 3. Black line: force–displacement curve of a standard push-out test; red dashed lines: maximum indentation depths of the stopped push-out tests. (For interpretation of the references to color in this figure legend, the reader is referred to the web version of this article.)

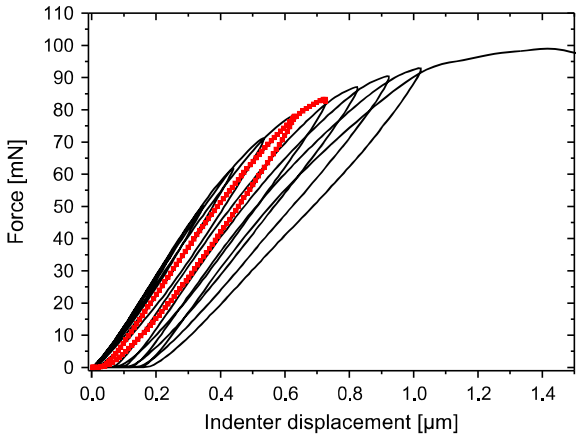

Fig. 4. Force–displacement curve of cyclic push-out test. For better visibility only the first 1.5 µm of indenter displacement are shown. Red: fourth cycle emphasized. (For interpretation of the references to color in this figure legend, the reader is referred to the web version of this article.)

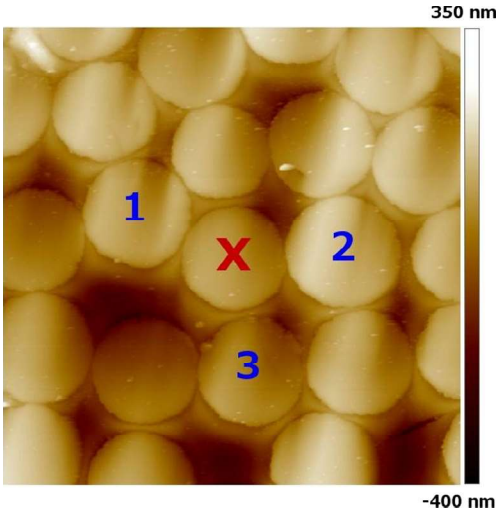

Fig. 5. AFM measurement of the front surface before the push-out test. Red cross: fiber investigated; blue numbers: reference fibers to identify the residual deformation; image size 30 µm × 30 µm. (For interpretation of the references to color in this figure legend, the reader is referred to the web version of this article.)

In Figs. 5 and 6 an exemplary AFM measurement of the front surface before and after push-out test is shown. For each stopped push-out test the residual deformations of the front and back surface are calculated as follows:

1. The relative deformation $\Delta z'$ on the front surface (back surface) of the fiber investigated (red crosses in Figs. 5 and 6) is calculated by subtraction of the height of the fiber after (z_{after}) and before (z_{before}) the stopped push-out test. The respective heights z are obtained by averaging the height values within the cross-section of the fiber investigated

$$\Delta z' = z_{after} - z_{before} \tag{1}$$

2. The reference height K is calculated by analyzing the mean height difference of 3 surrounding fibers after and before the test (blue numbers in Figs. 5 and 6). As above, the heights are obtained by averaging the height values of the respective fibers

$$K = \frac{\sum_{i=1}^{3}(z_{i,after} - z_{i,before})}{3} \tag{2}$$

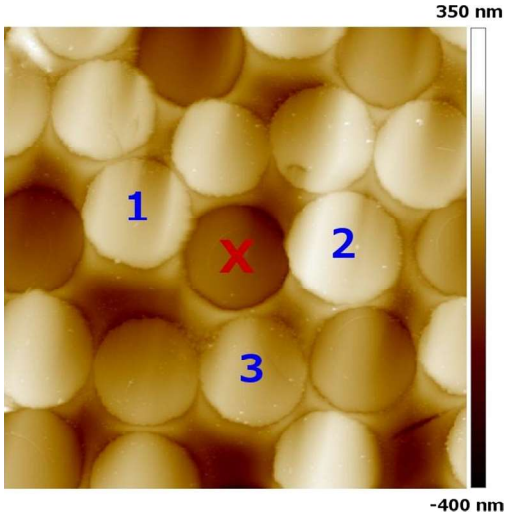

Fig. 6. Corresponding AFM measurement of the front surface after the push-out test with a maximum indentation depth of 800 nm. Red cross: fiber investigated; blue numbers: reference fibers to identify the residual deformation; image size 30 μm × 30 μm. (For interpretation of the references to color in this figure legend, the reader is referred to the web version of this article.)

3. The reported residual deformation on the front surface (back surface) is then calculated by subtracting the relative deformation on the front surface (back surface) and the reference height

$$\Delta z = \Delta z' - K \tag{3}$$

For push-out experiments performed with a flat cone indenter, fiber crushing is often a problem. The data presented in this paper is therefore only based on fibers, which have not been crushed during the measurement. This was verified by optical microscopy and atomic force microscopy of the front and back surface of the sample (cf. Figs. 6 and 7).

4. Finite element modeling

In order to assist the interpretation of the experimentally obtained force–displacement curves, a push-out experiment was numerically investigated using finite element modeling. All notations in the following refer to the usage in the structural mechanics module within Comsol version 4.4, which has been used for all calculations.

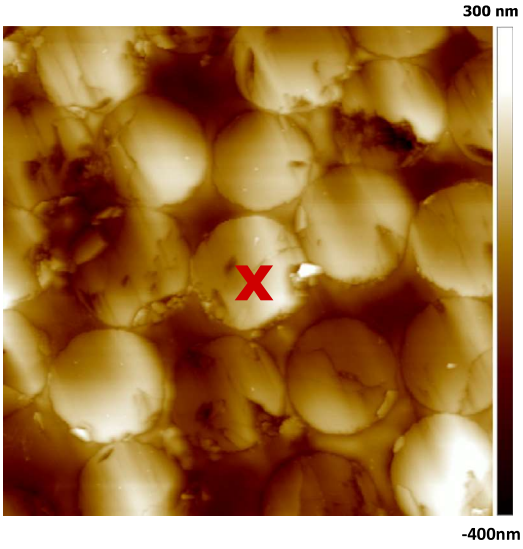

Fig. 7. AFM measurement of the back surface after the push-out test. Red cross: fiber investigated; image size 30 μm × 30 μm. (For interpretation of the references to color in this figure legend, the reader is referred to the web version of this article.)

To take into account the vicinity of the fiber under investigation, a full 3-dimensional representative model was developed. As shown in Fig. 8, the nearest neighbors of the fiber investigated were modeled and their spatial distances and diameters were extracted from microscopy images. To terminate the geometry an adjacent cuboid was modeled (Fig. 9). Edge constraints were chosen at the bottom of the model to simulate the support on the groove. The geometry of the indenter tip was modeled based on microscopy images and is placed on top of the fiber under investigation (Fig. 9). Material properties used are given in Table 1. We applied linear elastic material models for the diamond indenter tip and elastoplastic material models utilizing a work-hardening approach for the RTM6 polymer based on literature values [21]. We assume compressive yield strength of 3650 MPa for the orthotropic elastoplastic model of the carbon fiber utilizing an approach with perfect plasticity beyond 3650 MPa. The outer part of the sample uses a linear elastic orthotropic material model based on the macroscopically homogenized composite properties [21]. To model the interaction between carbon fiber and indenter tip, we apply a contact modeling approach. Since contact modeling of flat surfaces can inhibit numerical convergence, we decided to modify the surface geometry of the carbon fiber investigated. To stabilize the contact modeling calculation, a small curvature with 100 nm extension in z-direction was attached to the top of the fiber investigated. This is in accordance with the natural roughness of the carbon fibers after polishing as observed in AFM investigations.

To model the residual stresses due to the curing process at 180 °C we use isotropic thermal expansion coefficients for the RTM6 polymer and anisotropic thermal expansion coefficients for the fibers based on [22]. To this end, the thermal expansion setting was used assuring an initial stress state based on a cooling from the curing temperature of 180 °C to room temperature, i.e., a temperature difference of 157 °C.

Interfacial crack growth is modeled following the work of Rodriguez et al. [12] using an implementation for cohesive zone modeling in Comsol. The boundary condition "thin elastic layer" was chosen for the interface between fiber and matrix. The traction–separation law is formulated in terms of the stress at the interface σ

$$\sigma = \sqrt{\langle \sigma_n \rangle^2 + \tau_{t1}^2 + \tau_{t2}^2} \tag{4}$$

and the internal separation of the thin elastic layer nodes δ

$$\delta = \sqrt{\langle \delta_n \rangle^2 + \delta_{t1}^2 + \delta_{t2}^2} \tag{5}$$

with respect to normal (n) and transverse ($t1$, $t2$) directions. For the evaluation of the normal component the Macaulay brackets $\langle\rangle$ are used returning the argument if positive and zero if negative. This is used to allow crack propagation only for positive contributions of σ_n.

Following the recommendation of [12] we implemented a quadratic interaction criterion to derive the critical stress value R_c for crack initiation. This is written in terms of the critical interfacial strengths in normal (R_n) and transverse directions (R_{t1} and R_{t2}) as

$$\left(\frac{\langle \sigma_n \rangle}{R_n}\right)^2 + \left(\frac{\langle \tau_{t1} \rangle}{R_{t1}}\right)^2 + \left(\frac{\langle \tau_{t2} \rangle}{R_{t2}}\right)^2 = 1 \tag{6}$$

Following the considerations made in [12,25], we assume $R_{t1} = R_{t2}$ and R_n to be negligible for the present case. Therefore, Eq. (6) can be written solely in terms of one critical stress value R_c.

For numerical implementation we choose to rewrite Eq. (6) in terms of the internal separation of the layer nodes δ and use a

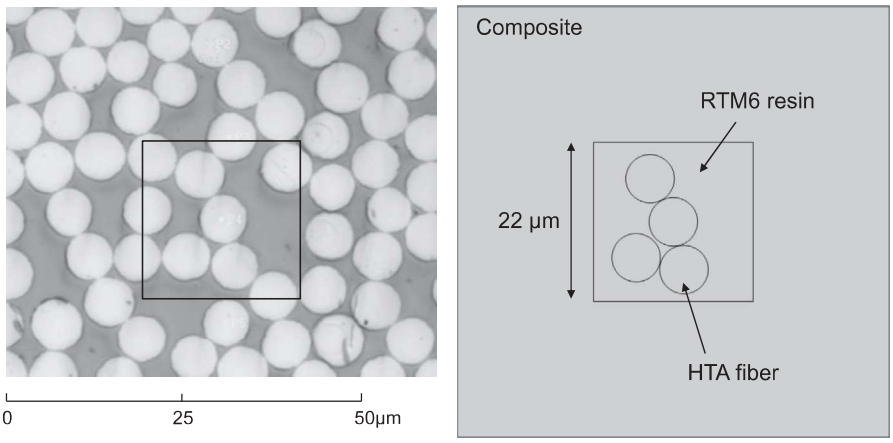

Fig. 8. Left: Microscopy image of the investigated fiber right: Two-dimensional model of the investigated fiber with spatial distances and geometries extracted from the microscopy image.

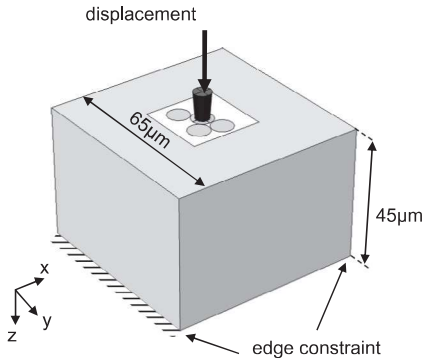

Fig. 9. Three dimensional model of a push-out test including edge constraints.

linear degradation rule after exceeding the peak value δ_{peak} of displacement.

For technical reasons, the Comsol environment also requires an additional ordinary differential equation to be defined on the fracture surface. This is to track the historic maximum value of δ. Therefore, the current implementation evaluates, whether the fracture condition is fulfilled in the present time step i or was fulfilled in any previous time step. Therefore we evaluate

$$\delta = \max\left(\delta[i],\ \delta[i-n]\right)\ \forall\ n \in [0, i] \tag{7}$$

Crack opening is then formulated as degradation of the stiffness vector $\vec{k}$ of the thin elastic layer nodes using a spatial degradation function $D(\vec{r})$

$$D(\vec{r}) = \begin{cases} 1 & \text{if} \quad \delta(\vec{r}) < \delta_{peak} \\ \frac{\delta_{peak}}{\delta_{break}-\delta_{peak}} \cdot \frac{\delta_{break}-\delta(\vec{r})}{\delta(\vec{r})} & \text{if} \quad \delta_{peak} \le \delta(\vec{r}) < \delta_{break} \\ 0 & \text{if} \quad \delta(\vec{r}) \ge \delta_{break} \end{cases} \tag{8}$$

The values for δ_{peak}, δ_{break} and the according interfacial fracture toughness are chosen to provide a best match to the experimental curves based on the experimentally deduced value of the interfacial fracture toughness of 90 J/m^2. The components of the initial stiffness vector $\vec{k}$ are chosen to be sufficiently high to avoid noticeable impact on the compliance of the full model.

For simulation of the push-out a transient simulation using a Generalized-α solver is applied. Initially, the residual stresses are calculated and an increasing displacement is applied to the top surface of the indenter tip. The calculation is carried out for 1 s using a displacement increase of 1000 nm/s. Force values are evaluated from the average stress on the top surface of the indenter tip that acts in z-direction.

For all calculations, we use linear order elements with a global mesh size below 10 µm. To resolve geometric details and the curvature of the geometries, the mesh was locally refined down to 0.5 µm. The sufficiency of these settings was validated by subsequent refinement of the mesh by factor of two. No differences in the calculated results were found.

5. Results and discussion

In the following results from experimental and simulated push-out tests of carbon fiber reinforced RTM6 epoxy resin are presented. First, experimental and simulated force–displacement curves and residual deformations are discussed. Then a new method for characterization of crack initiation and crack propagation is presented, which is based on cyclic push-out experiments and the evaluation of elastic and plastic energy contributions.

5.1. Experimental force–displacement curves

In Fig. 10 an experimental force–displacement curve recorded during single-fiber push-out of the investigated CFRP is shown. Deviation from linear behavior is observed at a displacement of around 330 nm (350 nm ± 43 nm if averaged over all experimentally obtained push-out data). After reaching the load maximum of 90 mN, a slow decrease of force follows. Complete debonding and push-out of the fibers, characterized by an abrupt load decrease, is found at a displacement of around 2000 nm. In contrast to most literature data [8,17,18,20], no push-out of the fibers occurs at the load maximum. For the sample investigated no friction effects can be observed after push-out, since at the moment of push-out, the velocity of the fiber is too high for the response time of the feedback control of the UNAT. Therefore, the indenter tip is not able to restore the contact to the fiber before reaching zero force (at approximately 6 µm).

The onset of nonlinearity in the force displacement curves, for our sample observed at an indenter displacement of 350 nm, is usually interpreted as crack initiation between fiber and matrix in the literature [7–11]. Other energy dissipative processes during push-out test, like a plastic deformation of fiber or matrix, are not considered. As polymeric matrix systems often show substantial ductile behavior, the occurrence of plastic deformations of the polymer during push-out test should be expected to show an

Table 1
Summary of elastic and elastoplastic properties used within the simulation.

	RTM 6 resin	HTA carbon fiber	RTM6/HTA composite	Diamond
Density	1140 (kg/m^3)	1760 (kg/m^3)	1550 (kg/m^3)	3515 (kg/m^3)
Elastic properties	E = 2.76 (GPa)	E_{11} = 235.0 (GPa) $E_{22} = E_{33}$ = 19.1 (GPa) G_{12} = 7.2 (GPa) $G_{23} = G_{31}$ = 24.0 (GPa) ν_{12} = 0.28 ν_{23} = 0.33 ν_{31} = 0.02	E_{11} = 163.0 (GPa) $E_{22} = E_{33}$ = 6.8 (GPa) $G_{12} = G_{31}$ = 3.5 (GPa) G_{23} = 2.7 (GPa) ν_{12} = 0.32 ν_{23} = 0.55 ν_{31} = 0.02	E = 1145.0 (GPa)
Elastoplastic properties	σ_y = 26.8 (MPa) $\sigma_h = \sigma_y$ 55.2 (MPa) × tanh(37.7 (MPa) × ε)	σ_y = 3650.0 (MPa)		
Poisson ratio	ν = 0.38	–		ν = 0.07
Thermal expansion coefficients	$\alpha = 65.2 \times 10^{-6}$	$\alpha_{11} = -0.4 \times 10^{-6}$ $\alpha_{22} = \alpha_{33} = 10.0 \times 10^{-6}$		
Source	[22]	[22]	[21]	[23,24]

impact on the resulting force–displacement curves. The clearly different shape of the force displacement curves of polymer and ceramic matrix composites (see Fig. 1) also supports this assumption.

5.2. Residual deformation

To elucidate the occurrence of plastic deformations of the polymer matrix, a microscopic investigation of residual deformations of the fiber–matrix system after different stages of the push-out test was performed. The residual deformations, as displayed in Fig. 11, have been quantified by AFM measurements. To this purpose the front and back surface of the sample were scanned after stopped push-out tests and the height differences between fiber and matrix were determined, as described above. These residual deformations can be caused by crack initiation between fiber and matrix with a push-in of the fiber or a plastic deformation of the matrix, since plastic deformation of the fiber was found to be negligible at these force levels (cf. Fig. 7). Despite the thorough AFM methodology described in Section 3.2, the error bars of the experimental data points indicate a relatively high uncertainty of the experimental values. Reasons can be small variations of the surface quality of the analyzed CFRP regions, varying surrounding of the analyzed fibers or deviation from the center position of the indenter on the fiber.

The AFM results show the onset of significant residual deformation on the front surface at indenter displacements of about 450 nm. With increasing indenter displacement up to 800 nm an increase in residual deformation up to 100 nm is observed. The onset of residual deformation is found at clearly higher indenter displacements than the deviation from linear behavior of the force displacement curve, located at 350 nm. In literature, the start of nonlinearity is generally interpreted as crack-initiation. However, in our case at the start of nonlinearity at 350 nm we do not observe a corresponding residual push-in of the fiber. The latter is surprising, since a partial debonding should lead to a redistribution of residual stresses and therefore cause some residual deformation. The residual deformation on the back surface starts at an indenter displacement between 600 nm and 700 nm, which is clearly higher than the indenter displacement for initiation of residual deformation on the front surface. At an indenter displacement of 600 nm, a residual deformation of about 20 nm is observed on the front surface, but no residual deformation is found on the back surface. Accordingly, it can be concluded, that stress concentration first occurs at the front side of the sample, before equivalent stress states are reached at the backside.

A continuous increase of residual deformation as function of indenter displacement is found for the CFRP sample, both on the front and the back surface. For brittle ceramic matrix systems a similar continuous increase of residual deformation of the front surface is found for comparable indenter displacements. However, during fiber push-in on ceramic matrix composites, no deformation on the back surface is observed [14]. The occurrence and the continuous increase of residual deformation of the back surface of our more ductile CFRP sample points to a plastic deformation of the polymer matrix.

5.3. Comparison of experimental and simulated force–displacement curves

To further support our understanding of the progress of push-out and the influence of elastic and plastic energy contributions on the force–displacement curves, a finite element simulation of the push-out process was performed following the method described in Section 5.

Fig. 12 shows a comparison between an experimental force–displacement curve (black) and simulation results obtained for different model configurations (colored). For all models, in the initial part a non-linear force–displacement response occurs, which is caused by the convex surface of the fiber and the respective formation of a full areal contact. This is accounted for in all models using the contact modeling approach described in Section 5.

Using solely linear elastic properties for matrix and fiber materials (blue curve), a linear slope is obtained above 100 nm indenter displacement. For more than 200 nm indenter displacement, an increasing deviation from the experimental curve is found. In this region purely linear elastic material models are obviously not sufficient to describe the experimental curve. One possible reason for the onset of the experimentally observed nonlinearity is the onset of crack growth at the interface between fiber and matrix, as demonstrated in Ref. [12]. Since the crack initiation at the interface affects the measured stiffness of the fiber–matrix system, this is likely to cause noticeable change of the force–displacement curve. Therefore we modeled the experimental configuration of Fig. 5 using δ_{peak} = 120 nm and δ_{break} = 1.5 µm to match the experimentally obtained fracture toughness value of 90 J/m^2 and a reasonable value of R_c = 120 MPa. The simulation result is shown in Fig. 12 (cyan curve). The simulation result shows an onset of nonlinear behavior due to crack growth at 545 nm. However, the curve is not sufficient to describe the experimental data. Also, a systematic reduction to δ_{peak} = 10 nm and δ_{break} = 1.0 µm simulating values of 5 J/m^2 interfacial fracture toughness and R_c = 10 MPa did not prove sufficient to describe the experimental curve. So crack initiation cannot explain the deviation of the force–displacement curve from linear behavior in the present case.

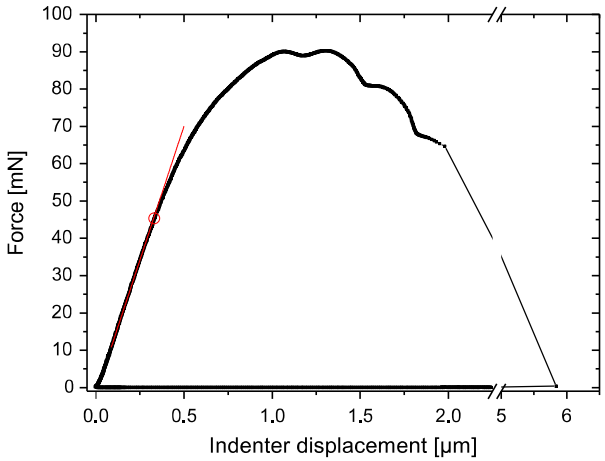

Fig. 10. Exemplary force–displacement curve of a push-out test. The deviation from linear behavior is marked with a red circle. (For interpretation of the references to color in this figure legend, the reader is referred to the web version of this article.)

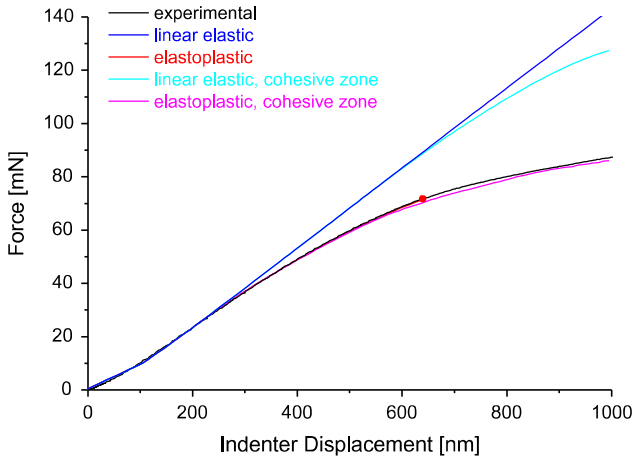

Fig. 12. Simulation of a standard push-out force–displacement curve with different material models; black: experimental curve, blue: linear elastic fiber and linear elastic matrix; cyan: linear elastic fiber and linear elastic matrix in combination with cohesive zone model, red: elastoplastic fiber and elastoplastic matrix; magenta: elastoplastic fiber and elastoplastic matrix in combination with cohesive zone model. (For interpretation of the references to color in this figure legend, the reader is referred to the web version of this article.)

Introducing an elastoplastic material law for fiber and matrix material yields the simulated force–displacement curve shown in red in Fig. 12. This curve fits the experimental data very well up to a displacement of about 560 nm. This demonstrates that the non-linearity of the force–displacement curve can be described by plastic deformation of the matrix surrounding the fiber. Beyond 560 nm, the model terminates (red dot in Fig. 12), since excessive plastic deformation of the matrix material cannot be calculated by the present formulation included in the model. Also, the evaluated stresses along the interface exceed the matrix material strength by more than one order of magnitude. Hence, the next model approach uses an elastoplastic formulation for fiber and matrix material and allows for crack growth at the interface between fiber and matrix using the values δ_{peak} = 120 nm and δ_{break} = 1.5 µm. The result is shown in Fig. 12 in magenta. The simulated force–displacement curve shows good agreement to the experimental curve. Therefore, the latter configuration is assumed to allow some further conclusions on the fiber push-out in our experiment. Firstly, the deviation of the force–displacement curve from linear behavior can be described by plastic deformation of the matrix material. Secondly, crack initiation at the fiber–matrix interface in the simulation starts at clearly higher indenter displacements of about 560 nm.

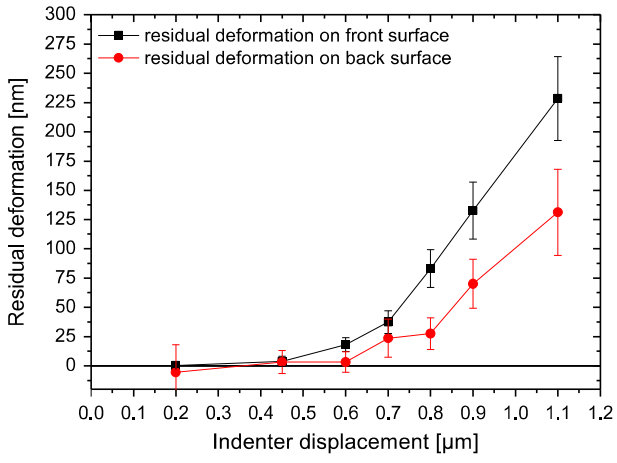

Fig. 11. Comparison of the residual deformation on the front and back surface measured by AFM. (For interpretation of the references to color in this figure legend, the reader is referred to the web version of this article.)

An evaluation of the degradation function $D(\vec{r})$ at the surface between fiber and matrix is shown in Fig. 13. The outline of the fiber and matrix geometry is added as reference frame. The first exceedance of δ_{peak} occurs at 450 nm causing first gradual degradation of the interfacial stiffness. Subsequently, the degradation intensifies along the narrow regions between fibers and also starts to grow in the circumferential direction. Until the maximum force, the interface degradation has almost fully grown to the backside, but has not yet fully developed at the interface, so the fiber is still not finally pushed out. In addition, some parts of the interface are fully degraded ($D(\vec{r}) = 0$) and therefore resemble the presence of a crack at this positions (cf. Fig. 13). For the progress of debonding along the interface the neighboring fibers have a significant impact. As seen in Fig. 13, there is distinct difference in the formation of the interfacial crack in the areas close to neighboring fibers and areas without neighboring fibers. Following Ref. [12] it is thus relevant to also consider the contribution of plasticity in these different regions. Therefore, the plastic deformation zone is plotted in Fig. 14. The color values show the effective plastic strain values exceeding a lower limit of 0.005. The plastic deformation zone initiates at the top surface, surrounding the pushed fiber, which is in accordance to the analysis of the residual deformations. The plastic deformation zone precedes the regions of interface degradation, which is caused by the elastoplastic material law and the choice of δ_{peak} and δ_{break} with respect to the linear elastic range of the matrix material. With increased loading the zone of plastic deformation grows along the fiber axis until it reaches the backside. Similar to the crack growth, high plastic deformation values concentrate in areas of narrow distance between neighboring fibers. At 450 nm indenter displacement, the plastic deformation zone already spans the whole thickness of the sample. At the same indenter displacement the onset of residual deformation on the front surface of the sample was detected by AFM (see Fig. 11). At higher indenter displacement values, zones of plastic deformation also appear at other locations than the interface of the fiber investigated.

5.4. Energy analysis during a push-out experiment

As suggested by the investigations described in Section 5.3, for the carbon fiber reinforced RTM6 epoxy resin the deviation from

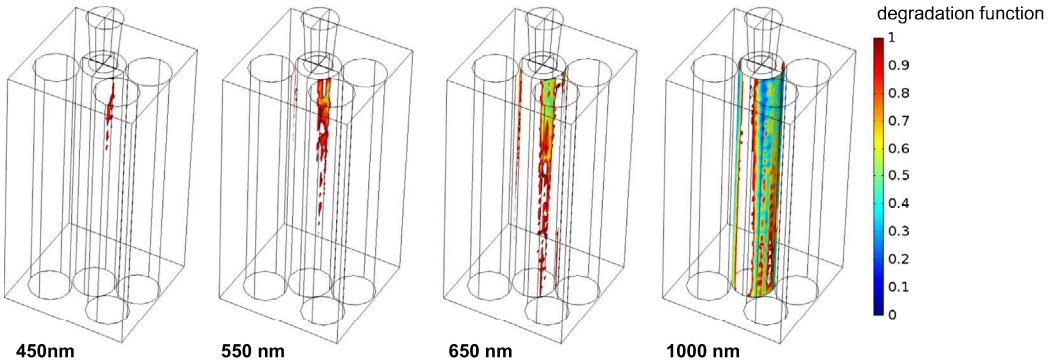

Fig. 13. Simulated crack growth states at 450 nm, 550 nm, 650 nm and 1000 nm indentation depth. Boundaries of geometric elements are shown as reference frame. Color values show values of degradation function (values above 0.99 were chosen transparent). Complete debonding is observed for $D(\vec{r}) = 0$. (For interpretation of the references to color in this figure legend, the reader is referred to the web version of this article.)

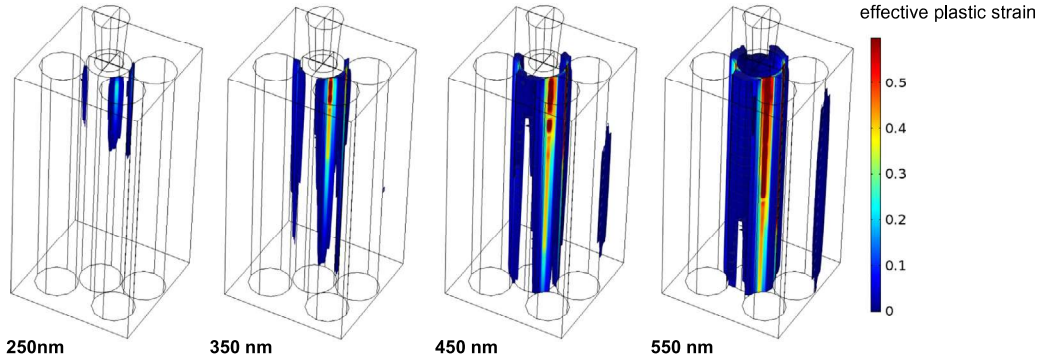

Fig. 14. Simulated plastic deformation states at 250 nm, 350 nm, 450 nm and 550 nm indentation depth. Boundaries of geometric elements are shown as reference frame. Color values show effective plastic strain values (values below 0.005 were chosen transparent). (For interpretation of the references to color in this figure legend, the reader is referred to the web version of this article.)

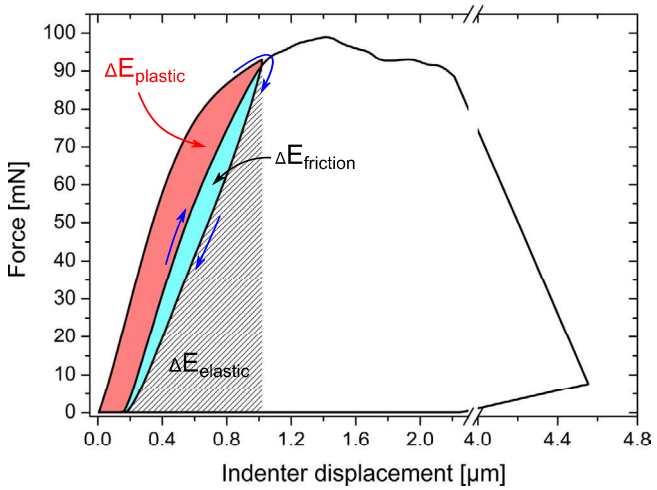

Fig. 15. Force–displacement curve of a push-out test including one unloading–loading cycle at 1 µm. The corresponding elastic energy is black hatched, the work of friction cyan and the plastic energy red. (For interpretation of the references to color in this figure legend, the reader is referred to the web version of this article.)

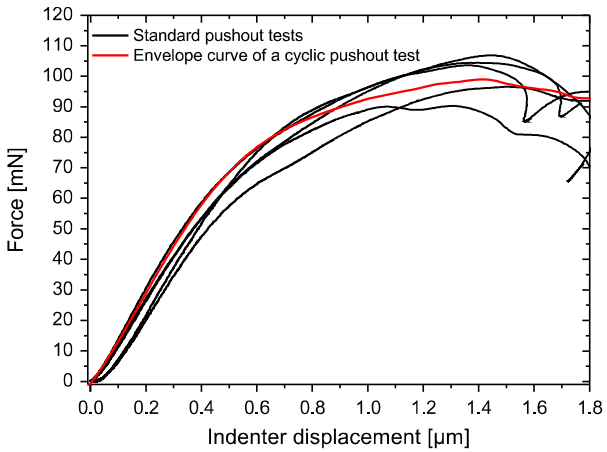

Fig. 16. Comparison of the envelope curve of a cyclic push-out test (red) to standard push-out curves (black). (For interpretation of the references to color in this figure legend, the reader is referred to the web version of this article.)

linear behavior of the push-out force–displacement curve is unlikely to indicate crack initiation at the fiber–matrix interface.

Therefore, we adopted an experimental approach using cyclic loading to retrieve the different energy contributions during a push-out experiment [14,25,27]. Compared to quasi-static push-out experiments, this comprises a cyclic loading of the fiber with unloading–loading cycles. The contributions of elastic, plastic and other dissipative energies can then be calculated from the different areal fractions between the loading and unloading curves. Fig. 15 shows an example of a force–displacement curve with one unloading–loading cycle at an indenter displacement of 1 µm. The total energy deposited in the system corresponds to the integral of the force displacement curve up to the indenter displacement of 1 µm, which is equivalent to the sum of elastic, plastic and dissipative

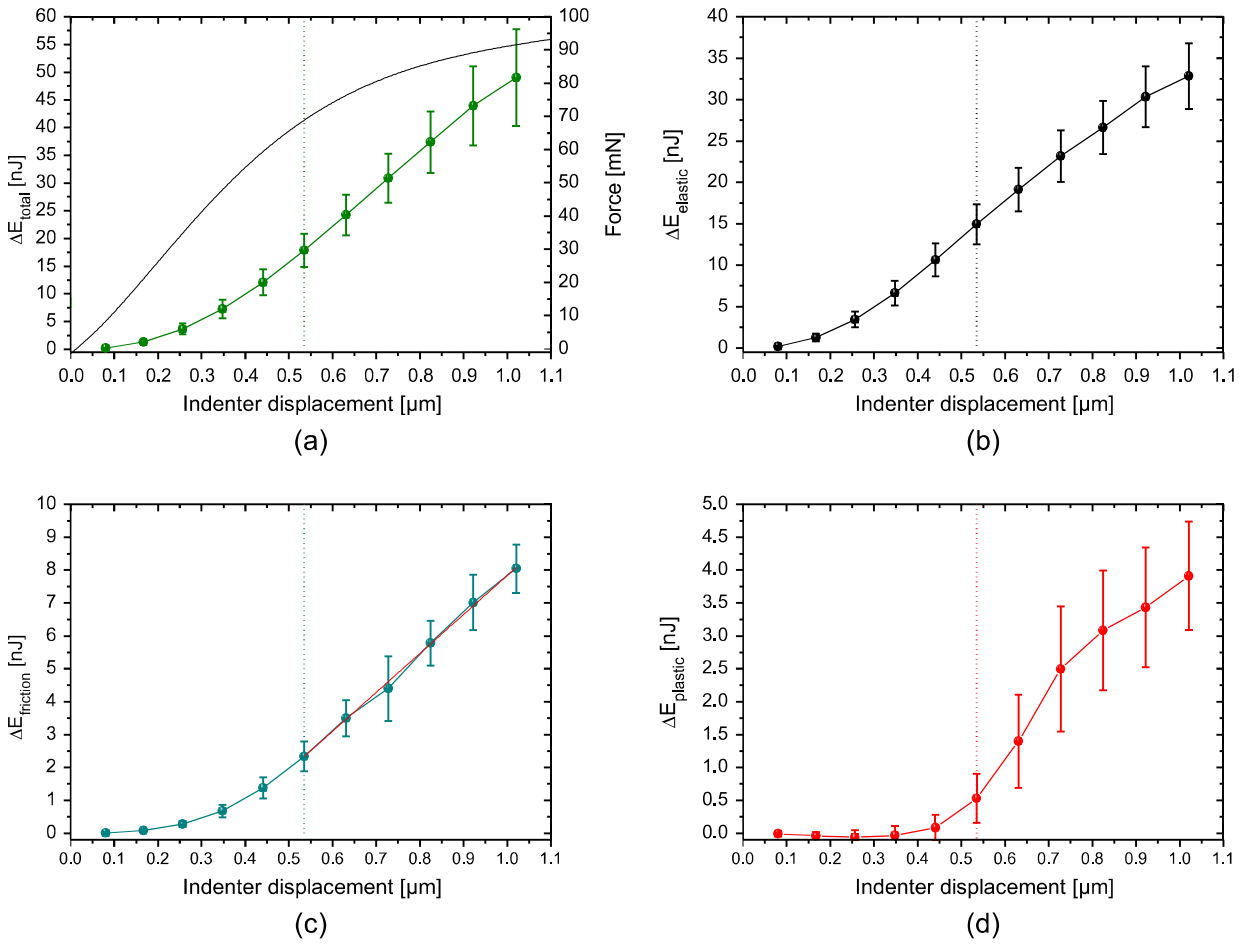

Fig. 17. Mean values and standard deviation of (a) the total energy per cycle together with an exemplary force displacement curve, (b) the elastic energy per cycle, (c) the work of friction per cycle, and (d) the plastic energy per cycle. (For interpretation of the references to color in this figure legend, the reader is referred to the web version of this article.)

energy contributions. The elastic energy deposited in the system is released upon unloading and is equivalent to the area below the unloading curve (black hatched). All dissipative energies thus correspond to the area between the initial loading and the unloading curve. Upon reloading, the force–displacement curve is different to the previous unloading curve, which was at first attributed to frictional sliding between fiber and matrix [26], but was previously generalized to work of friction to account for all frictional terms during the measurement [14,27]. So the difference in the loading curves allows for distinction between the plastic energy contribution (red) and the work of friction (cyan). To measure the progress of the different energy contributions during a push-out test, multiple unloading–loading cycles are performed every 100 nm of indenter displacement.

It is worth noting that the modification of the standard push-out test to a cyclic one does not affect the shape of the push-out curve and the damage progression should be similar. This equivalency is demonstrated by comparison of the envelope curve of a cyclic push-out test to the force–displacement curves of standard push-out tests (Fig. 16).

Fig. 17 shows the total energy (a), the elastic energy (b), the work of friction (c) and the plastic energy (d) spent per cycle as function of the indenter displacement of a cyclic push-out test. In the following, the evolution of the different energy contributions during a push-out experiment will be discussed.

Up to an indenter displacement of 100 nm almost no energy is dissipated in the system (Fig. 17a). Thus the nonlinear initial part of the force–displacement curve contains only small energy consuming processes like establishing a full contact between indenter and fiber. For larger displacements the total energy per cycle continuously increases with increasing displacement and no irregularities are observed. The strongest increase in total energy per cycle is found beyond an indenter displacement of about 540 nm (dashed line in Fig. 17) but cannot be associated with a particular signature in the force–displacement curve.

The elastic energy per cycle also increases continuously with the displacement (Fig. 17b). This is not surprising since the sample is increasingly deformed and therefore an increasing elastic deformation of the fiber matrix system is expected as well. The inflection point of the elastic energy per cycle curve is found at 540 nm (dashed line) and indicates a change in stiffness of the system, which could be indicative for crack initiation at the fiber–matrix interface and subsequent crack growth.

The first significant contribution of work of friction per cycle occurs at an indenter displacement of about 170 nm which is far before any plastic deformation occurs (compare Fig. 17c and d). So work of friction does not only account for fiber–matrix friction in previously debonded zones, but also any further frictional effects like friction in the measurement device itself or friction between indenter and fiber. Work of friction per cycle strongly increases beyond an indenter displacement of about 350 nm and is nearly linear beyond 540 nm (dashed line). In this linear part, the contribution of friction between the debonded fiber and the surrounding matrix is likely to dominate the work of friction contribution.

The first measurable plastic energy contribution per cycle is found beyond an indenter displacement of about 450 nm

(Fig. 17d), which is in good agreement with the start of residual deformation on the front surface of the sample (see Fig. 11). The simulation results indicate plastic deformation of the matrix to start already at 200 nm, but the corresponding plastic energy per cycle seems to be too small to be measurable. Beyond 540 nm (dashed line) a strong increase of plastic energy is observed. Here a substantial change of the behavior of the fiber–matrix system seems to occur. At an indenter displacement of about 750 nm a kink in the plastic energy curve is observed. For higher indenter displacements the plastic energy contributions show a nearly linear increase.

For further evaluation of the plastic energy contribution, the total plastic energy dissipated in the system (i.e., the accumulated plastic energy) up to the given indenter displacements is investigated (see Fig. 18). This plastic energy can be due to plastic deformation of the fiber, plastic deformation of the matrix, crack initiation or crack propagation. As quantified by AFM, plastic deformation of the fiber itself is negligible at these moderate force levels. Up to an indenter displacement of 300 nm only little plastic energy is dissipated in the system. Beyond 300 nm, there is a slight increase of the total plastic energy with a strong increase beyond 630 nm. This increase shows a linear behavior starting at a displacement of about 700 nm. Beyond 700 nm a linear increase of the total plastic energy is observed. This linear increase is attributed to a stable energy consuming process. Since there is no sudden change in the evaluated total plastic energy, which could be attributed to sudden increase in plastic deformation, in our opinion the only possibility for the observed stable dissipative energy contribution beyond an indenter displacement of 700 nm is stable crack propagation. Accordingly, the moment of crack initiation can be derived from the indenter displacement, where this contribution vanishes. Therefore, we conclude, that this is equivalent to the back-extrapolation to zero total plastic energy using a linear regression of the data points beyond 700 nm. This was evaluated to correspond to an indenter displacement of 588 ± 40 nm (blue shaded in Fig. 18) for the fiber–matrix system investigated. It is also in accordance with the strongest increase of total energy and the position of the inflection point of the elastic energy at 540 nm and the change in trend of the work of friction. Hence, these signatures indicate a change in the mechanical response of the specimen and therefore are strong indications for the moment of crack initiation. The rise of the total plastic energy at indenter displacements below crack onset can be attributed to plastic deformation of the matrix, which is confirmed by the simulation results and the residual deformations of the fiber–matrix system.

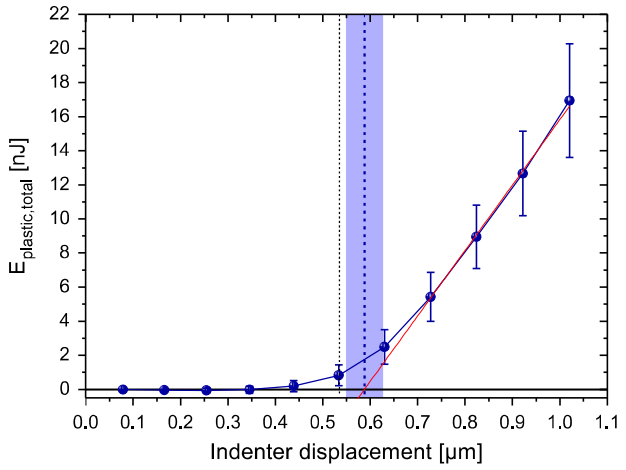

Fig. 18. Mean values and standard deviation of the total plastic energy. Red line shows fit of the linear behavior of the plastic energy beyond a displacement of about 0.7 µm. Extrapolation of the linear regression reaches zero energy at 588 nm ± 40 nm (blue shaded). (For interpretation of the references to color in this figure legend, the reader is referred to the web version of this article.)

There are no signatures in the force–displacement curves like deviation from linear behavior, a kink, or a plateau, indicating crack initiation. However, the evaluation of the energy contributions obtained by cyclic push-out tests allows determining the moment of crack initiation and the according plastic energy release independent of such signatures. Also, the described procedure does not require any assumptions on the material behavior but is solely based on the experimental data and is thus suitable for evaluation of different material systems as demonstrated by [27].

In particular, for the RTM6 epoxy material studied herein the deviation of the force–displacement curve from linearity at about 350 nm displacement, often interpreted as crack opening [7–11,17], does not indicate crack initiation but initiation of plastic deformation of the matrix.

6. Conclusions

We have presented a new method to evaluate the force–displacement curve of a single-fiber push-out test.

It has been shown that a deviation in the force–displacement curve from linear behavior in a push-out experiment of carbon fiber reinforced resin can be attributed to plastic deformation of the matrix rather than crack initiation. For the investigated carbon fiber reinforced RTM6 epoxy resin system plastic deformation is preceding crack initiation significantly.

AFM measurements of the residual deformation showed that a single-fiber push-out test is associated with significant plastic deformation of the surrounding matrix. Associated finite element modeling confirmed this result. Residual deformation on the back surface occurs after residual deformation on the front surface which indicates, that the deformation and the stress first concentrate at the front surface before they reach the backside. Therefore, crack initiation also occurs at the front surface which was confirmed by simulation. A slow, continuous increase of residual deformation is observed for moderate indenter displacements. Despite the fact that the crack did not reach the backside of the sample yet, a distinct residual deformation on the back surface occurs due to plastic deformation of the matrix.

The standard push-out test was modified by additional loading–unloading cycles, to allow the determination of the contributions of elastic, plastic and frictional energy during a push-out experiment. The total plastic energy increases linearly as soon as the energy release of crack propagation starts to dominate the energy dissipation. The indenter displacement obtained by backwards extrapolation of the linear range of the total plastic energy to zero is interpreted as the moment of crack initiation. This agrees well with the crack initiation derived from simulation results. The linear increase of total plastic energy and work of friction after crack initiation are both indicative of stable energy dissipation such as crack growth.

The results underline the importance of plastic deformation in carbon fiber reinforced polymers. The force–displacement curves of the CFRP samples analyzed are clearly affected by plastic deformation of the matrix material. For ductile matrix materials like RTM6, an interpretation of push-out data should, therefore, include such contributions of plastic deformation. For such matrix systems a deviation from linear behavior is not indicative of crack opening. Here an energy analysis is necessary to identify the dissipative energy contributions related to interfacial failure. For brittle matrix materials like some prepreg polymer types the effect of resin plasticity is expected to be less important and fiber decohesion might be observed before significant plastic deformation of the matrix

occurs. However, the presented experimental method does not depend on assumptions regarding the stress distribution along the fiber–matrix interface or the ductility of the matrix material and is in principle applicable to all fiber–matrix systems.

References

[1] DiFrancia C, Ward TC, Claus RO. The single-fiber pull-out test: 1: Review and interpretation. Composites Part A 1996;27:597–612.

[2] Nairn JA. Analytical fracture mechanics analysis of the pull-out tests including the effects of friction and thermal stresses. Adv Compos Lett 2000;9:373–83.

[3] Zhandarov S, Mäder E, Yurkevich OR. Indirect estimation of fiber/polymer bond strength and interfacial friction from maximum load values recorded in the microbond and pull-out tests. Part I: Local bond strength. J Adhes Sci Technol 2002;16:1171–200.

[4] Mendels D-A, Leterrier Y, Manson J-AE. The influence of internal stresses on the microbond test–I: Theoretical analysis. J Compos Mater 2002;36:347–63.

[5] Dilsiz N, Wightman JP. Effect of acid-base properties of unsized and sized carbon fibers of fiber/epoxy matrix adhesion. Colloid Surf, A 2000;164:325–36.

[6] Paipetis A, Galiotis C. A study of the stress–transfer characteristics in model composites as a function of material processing, fibre sizing and temperature of the environment. Compos Sci Technol 1997;57:827–38.

[7] Ramanathan T, Bismarck A, Schulz E, Subramanian K. Investigation of the influence of surface-activated carbon fibres on debonding energy and frictional stress in polymer-matrix composites by the micro-indentation technique. Compos Sci Technol 2001;61:2511–8.

[8] Sha JJ, Dai JX, Li J, Wei ZQ, Hausherr J-M, Krenkel W. Measurement and analysis of fiber-matrix interface strength of carbon fiber-reinforced phenolic resin matrix composites. J Compos Mater 2013. http://dx.doi.org/10.1177/0021998313485264.

[9] Kharrat M, Chateauminois A, Carpentier L, Kapsa P. On the interfacial behavior of a glass/epoxy composite during a micro-indentation test: assessment of interfacial shear strength using reduced indentation curves. Composites Part A 1997;28:39–46.

[10] Molina-Aldareguia JM, Rodriguez M, Gonzalez C, LLorca J. An experimental and numerical study of the influence of local effects on the application of the fibre push-in test. Philos Mag 2011;91:1293–307.

[11] Zidi M, Carpentier L, Chateauminois A, Sidoroff F. Quantitative analysis of the micro-indentation behavior of fibre-reinforced composites: development and validation of an analytical model. Compos Sci Technol 2000;60:429–37.

[12] Rodriguez M, Molina-Aldareguia JM, Gonzalez C, LLorca J. A methodology to measure the interface shear strength by means of the fiber push-in test. Compos Sci Technol 2012;72:1924–32.

[13] Kalinka G, Leistner A, Hampe A. Characterisation of the fibre/matrix interface in reinforced polymers by the push-in technique. Compos Sci Technol 1997;57:845–51.

[14] Mueller WM, Moosburger-Will J, Sause MGR, Horn S. Microscopic analysis of single-fiber push-out tests on ceramic matrix composites performed with Berkovich and flat-end indenter and evaluation of interfacial fracture toughness. J Eur Ceram Soc 2013;33:441–51.

[15] Hinoki T, Zhang W, Kohyama A, Sato S, Noda T. Effect of fiber coating on interfacial shear strength of SiC/SiC by nano-indentation technique. J Nucl Mater 1997;258–263:1567–71.

[16] Sha J, Hausherr J-M, Krenkel W. Characterization of fiber–matrix interface bonding at the cfrp step of fiber fabrication process by single fiber push-out technique. Verbundwerkstoffe: 17 Symp Verbundwerkstoffe und Werkstoffverbunde 2009;202–209. http://dx.doi.org/10.1002/9783527627110.ch28.

[17] Chandra N, Ghonem H. Interfacial mechanics of push-out tests: theory and experiments. Composites Part A 2001;32:575–84.

[18] Guichet B, Sangleboeuf J-C, Vassel A, Bretheau T. Study of push-out micromechanical test: response of SCS-6/Ti-6242 composite. Key Eng Mater 1998;127–131:651–8.

[19] Sharma R, Mahajan P, Mittal RK. Fiber bundle push-out test and image-based finite element simulation for 3D carbon/carbon composites. Carbon 2012;50:2717–25.

[20] Li X, Yang Q, Liu Z. Interfacial mechanics of fiber push-out test: nano-indentation technique and cohesive element modeling. In: 13th International conference on fracture; 2013.

[21] Hobbiebrunken T, Hojo M, Fiedler B, Tanaka M, Ochiai S, Schulte K. Thermomechanical analysis of micromechanical formation of residual stresses and initial matrix failure in CFRP. JSME Int J Ser A 2004;47:349–56.

[22] Hobbiebrunken T, Fiedler B, Hojo M, Ochiai S, Schulte K. Microscopic yielding of CF/epoxy composites and the effect on the formation of thermal residual stresses. Compos Sci Technol 2005;65:1626–35.

[23] Reeber RR, Wank K. Thermal expansion, molar volume and specific heat of diamond from 0 to 3000 K. J Electron Mater 1996;25:63–7.

[24] McSkimin HJ, Andreatch P. Elastic moduli of diamond as a function of pressure and temperature. J Appl Phys 1972;43:2944.

[25] Battisti A, Esqué-de los Ojos D, Ghisleni R, Brunner AJ. Single fiber push-out characterization of interfacial properties of hierarchical CNT–carbon fiber composites prepared by electrophoretic deposition. Compos Sci Technol 2014;95:121–7.

[26] Marshall DB, Oliver WC. Measurement of interfacial mechanical properties in fiber-reinforced ceramic composites. J Am Ceram Soc 1987;70:542–8.

[27] Greisel M, Jäger J, Moosburger-Will J, Sause MGR, Mueller WM, Horn S. Influence of residual thermal stress in carbon fiber-reinforced thermoplastic composites on interfacial fracture toughness evaluated by cyclic single-fiber push-out tests. Composites Part A 2014;66:117–27.